RESEARCH ARTICLE

Evaluation of layout and atmospheric stability effects in wind farms using large-eddy simulation

Niranjan S. Ghaisas[1] [iD], Cristina L. Archer[1], Shengbai Xie[1], Sicheng Wu[1] and Eoghan Maguire[2]

[1] College of Earth, Ocean, and Environment, University of Delaware, Newark, Delaware, USA
[2] Research and Development, Vattenfall, Edinburgh, UK

ABSTRACT

Large-eddy simulation (LES) has been used previously to study the effect of either configuration or atmospheric stability on the power generated by large wind farms. This is the first study to consider both stability and wind farm configuration simultaneously and methodically with LES. Two prevailing wind directions, two layouts (turbines aligned versus staggered with respect to the wind) and three stabilities (neutral and moderately unstable and stable) were evaluated. Compared with neutral conditions, unstable conditions led to reduced wake losses in one configuration, to enhanced wake losses in two and to unchanged wake losses in one configuration. Conversely, stable conditions led to increased wake losses in one, decreased wake losses in two and unchanged wake losses in one configuration. Three competing effects, namely, rates of wake recovery due to vertical mixing, horizontal spread of wakes and localized regions of acceleration caused by multiple upstream wakes, were identified as being responsible for the observed trends in wake losses. The detailed flow features responsible for these non-linear interactions could only be resolved by the LES. Existing analytical models ignore stability and non-linear configuration effects, which therefore need to be incorporated. Copyright © 2017 John Wiley & Sons, Ltd.

1. INTRODUCTION

The vertical distribution of temperature affects heat and momentum exchanges in the atmospheric boundary layer (ABL). As a result, vertical motion and turbulent mixing can be enhanced, inhibited or unaffected and the atmosphere is defined unstable (or convective), stable or neutral, respectively. Neutral stability occurs in adiabatic conditions (i.e., without heat exchanges) and is the most common assumption in studies of flow around wind turbines. Compared with neutral, unstable conditions are characterized by high levels of turbulent kinetic energy (TKE), while stable conditions usually have lower TKE. In stable conditions, a low-level jet often forms near the rotors of wind turbines, impacting wind power generation because of strong wind shear. Because of these complicating factors, the effect of atmospheric stability on the power harvested by wind farms is unclear.

Past field campaigns reflect these complexities and point to conflicting trends in the impact of atmospheric stability on power production. Wharton and Lundquist[1] observed increased power for stable over neutral and unstable conditions, while Vanderwende and Lundquist[2] and Wharton *et al.*[3] observed increased power for unstable over neutral and stable conditions in actual wind farms. Drawing unambiguous conclusions about the role of stability from field observations is difficult because of numerous additional factors, such as variable wind speed, direction and shear; turbulent intensity levels; and geostrophic forcing. Well-controlled numerical experiments can be useful in clarifying the role of atmospheric stability. There have been several studies on incorporation of atmospheric stability effects in simplified wake models. For example, observations of stability effects in the HornsRev wind farm and evaluation of several wake models were reported

in Hasager and Giebel,[4] while Peña *et al.*[5] proposed changes to the wake expansion coefficient in the classical PARK wake model on the basis of these observational data. As noted by Peña and Rathmann,[6] comparing predictions of wake models with observations is complicated by the need to process the observations themselves, which is challenging. Numerical simulations provide high-fidelity data that can also be used for evaluation and development of wake models.

Some recent studies used numerical simulations to examine the influence of stability on wind turbine/farm performance. However, these studies considered either a single turbine[7–9] or infinitely large wind farms with periodic boundary conditions in the horizontal directions.[10–12] The effect of stable, neutral and unstable conditions with the same hub-height velocity across simulations was studied for an isolated, single turbine by Abkar and Porté-Agel.[9] Their analysis focused on the characteristics of turbulent wakes and did not describe interactions between multiple wakes or the expected power output. The effect of increasing stable stratification of the ABL on the flow characteristics in an infinitely large wind farm was investigated using large-eddy simulations (LES) by Abkar and Porté-Agel.[11] The power was found to be impacted significantly (up to 35%) for the stratification levels studied. A similar LES study by Lu and Porté-Agel[12] quantified the effect of an infinitely large wind farm on the ABL under convective conditions. Both these studies used periodic boundary conditions on the horizontal boundaries, thus assuming that the wind farms were infinitely large, and the ABL was fully developed. To the best of our knowledge, there are no LES studies on the effects of stability in realistic (i.e., large but finite) wind farms.

Apart from atmospheric stability, the power production of wind farms is affected significantly by the layout of turbines.[13,14] In our previous study,[13] a number of layouts obtained by staggering alternate rows and/or increasing the spacing in streamwise and spanwise directions, with respect to a control layout, were evaluated and the differences in array losses and power production were found to vary from 13% to 33%. The Lillgrund offshore wind farm,[15,16] comprising 48 Siemens 2.3 MW turbines, was the control layout. Neutral atmospheric stability was assumed for all simulations, and only one direction, corresponding to the prevailing southwesterly wind direction (225° following the meteorological convention), was investigated. The second prevailing wind direction at Lillgrund is northwesterly (315°).

In this paper, 12 LES are carried out, covering two layouts (original Lillgrund and staggered), two wind directions (225° and 315°) and three stabilities (neutral, unstable and stable). Our goals are to identify and quantify the effects of layout, wind direction and stability on the performance of wind farms. This paper is structured as follows. The numerical methodology, validation of the solver and a description of the cases simulated is provided in Section 2. The combined effect of wind farm layout, direction and stability on the power generation and the flow structures are presented in Section 3. The main conclusions are summarized in Section 4.

2. METHODOLOGY

2.1. Code description

The flow was governed by the LES-filtered continuity, momentum and potential temperature equations, described in detail by Archer *et al.*[13] The momentum equations included a uniform pressure gradient driving the flow, Boussinesq-buoyant and Coriolis forces, subgrid-scale (SGS) terms and actuator line model terms that model the body forces due to the wind turbine blades. All parameters in the simulations reported here were identical to those in Archer *et al.*[13]

The SGS stresses were modeled with the classical Smagorinsky model with coefficient $C_S = 0.13$ in the neutral and unstable cases. To accurately account for the reduced and intermittent nature of turbulence in stable cases, we used the Lagrangian-dynamic model[17] for the stable cases. A constant SGS Prandtl number of $1/3$ was used to model the SGS heat flux in the filtered potential temperature equation.

Since molecular viscosity and diffusivity were neglected, the stresses close to the ground were supplemented by wall models[18,19] based on the Monin–Obukhov similarity theory (MOST), as described in Abkar and Porté-Agel.[9]

The OpenFOAM-based numerical code simulator for on/offshore wind farm applications (SOWFA), developed by the National Renewable Energy Laboratory (NREL), was used for the simulations.[20–22] The equations were discretized using a second-order finite-volume scheme, and the solution was advanced in time using a second-order pressure implicit splitting operation algorithm with a predictor step followed by three corrector steps. Numerical and implementation details may be found in Churchfield *et al.*[20] and Churchfield.[23] We refer to Section 2.2 for detailed comments on the validation of the SOWFA code.

2.2. Validation of SOWFA solver

Comments about the validation of the SOWFA code are presented here. The SOWFA code has been validated previously for ABL flows under neutral and unstable conditions.[20,21] The logarithmic law of the wall under neutral conditions and the deviation from the logarithmic profile along with large-scale energetic structures under unstable conditions were accurately

simulated in Churchfield *et al.*[20] The windplant portion of SOWFA has been validated by its success at reproducing the power generated and the array losses in the Lillgrund wind farm.[21]

The stable version of SOWFA was introduced recently by Churchfield *et al.*[22] and has been used previously for ABL and windplant simulations by Bhaganagar and Debnath.[7,8] In order to validate the stable version, we performed simulations and reproduced results of (1) the stable ABL described in the GABLS intercomparison study Beare *et al.*[24] and (2) a single turbine immersed in the stable ABL (with periodic conditions to simulate an infinitely large windplant), corresponding to the study by Lu and Porté-Agel.[10] Details of these validation studies are presented as follows.

A stable ABL was set up in a domain of size $560 \times 560 \times 400$ m in the three Cartesian directions by reducing the temperature at the ground at the rate of -0.25 K h^{-1} starting from the reference temperature of 265 K. The domain was discretized in $100 \times 100 \times 60$ grid points in the three directions, and periodic conditions were maintained at all lateral boundaries. The simulations were carried out for 9 h, and time and horizontal averaging was performed over the last 1 h. These time-averaged and horizontal-averaged results are presented in Figure 1. Two LES SGS models were used: the constant-coefficient Smagorinsky model with $C_S = 0.13$ and the Lagrangian-averaging scale-invariant (LASI) dynamic model. The results are compared with the GABLS intercomparison study documented in Beare *et al.*[24] and a similar study by Lu and Porté-Agel.[10]

Figure 1(a) shows that the mean velocities are in excellent agreement with the results of Lu and Porté-Agel.[10] The profiles of U and V are rotated by approximately 20°, as noted in Lu and Porté-Agel.[10] Figure 1(b) shows that the same result without rotation lies within the spread displayed by the various studies in the GABLS intercomparison study. The mean temperature, TKE and momentum and buoyancy fluxes were comparable with the results of Lu and Porté-Agel,[10] and the GABLS simulations. Further, the LASI and constant-coefficient Smagorinsky LES models showed very similar results.

Lu and Porté-Agel[10] placed a turbine with diameter $d = 112$ m and hub-height 119 m, rotating at a constant 8 rpm, in the stable ABL described earlier. Periodic conditions were maintained at the lateral boundaries so as to simulate an infinitely large wind farm. Horizontal and time averages computed for 15 min following an initial transient of 45 min are compared in Figure 2. The mean velocities, temperature and the momentum and buoyancy fluxes are again seen to be in good agreement with the reference LES results. Note that exact agreement is not expected since three different LES are being compared. The LASI and constant-coefficient Smagorinsky model results were, again, very similar to each other.

Time-averaged results (without horizontal averaging) $1d$ to $4d$ downstream of the turbine are presented in Figure 3. The mean U velocities are seen to be in very good agreement between the three LES simulations. Note that each subplot in Figure 3(a) shows the precursor U profiles in addition to the profiles at a downstream location. Figure 3(b) shows
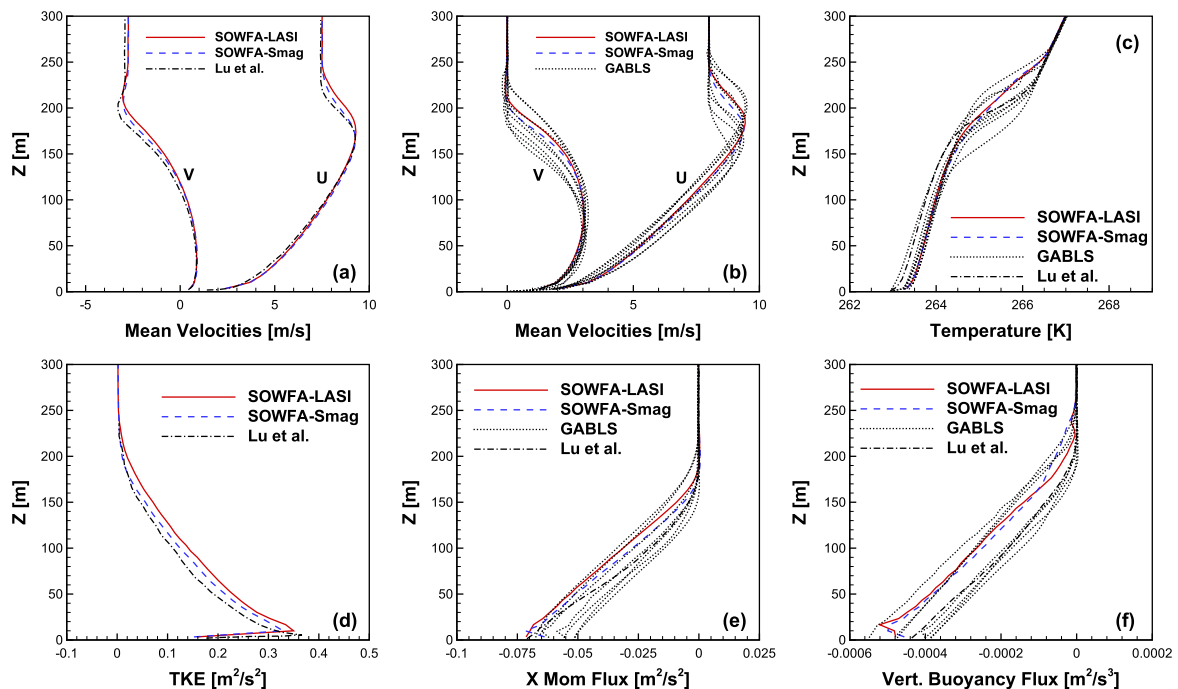

Figure 1. Stable precursor ABL LES results. (a) and (b) Mean velocities, (c) mean temperature, (d) TKE, (e) horizontal momentum flux, $\langle u'w' \rangle$ and (f) buoyancy flux, $g\langle w'\theta' \rangle / \theta_0$. Velocities in (a) are rotated by approximately 20°, following Lu and Porté-Agel.[10]
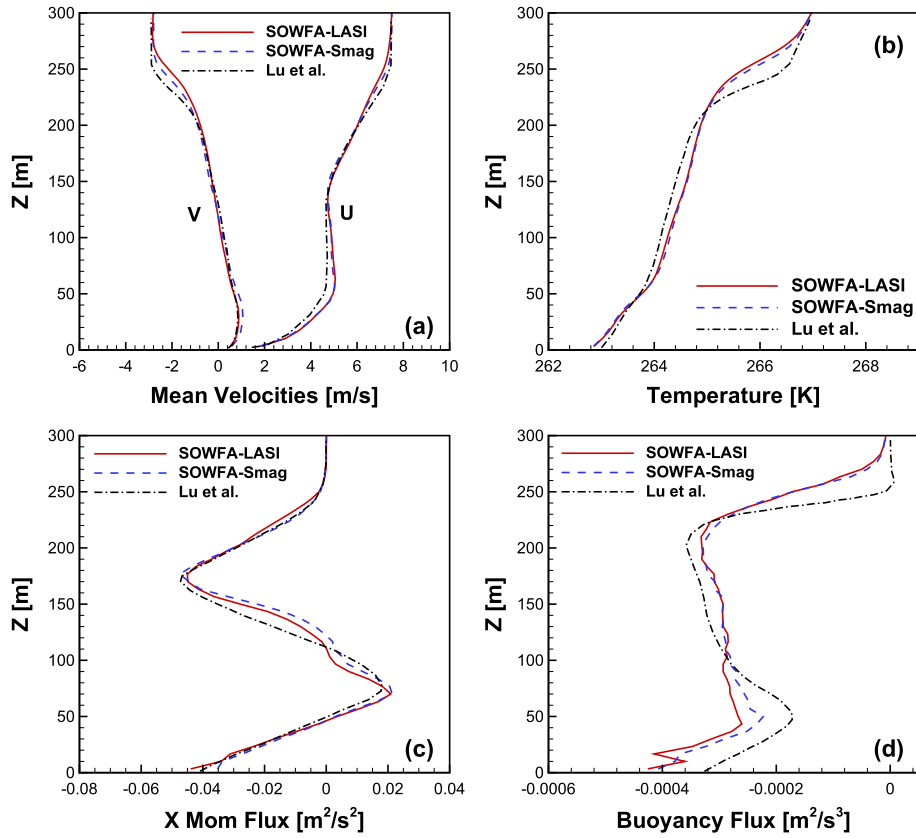
Figure 2. Horizontally averaged stable windplant LES results. (a) Mean velocities, (b) mean temperature, (c) horizontal momentum flux and (d) buoyancy flux. [Colour figure can be viewed at wileyonlinelibrary.com]
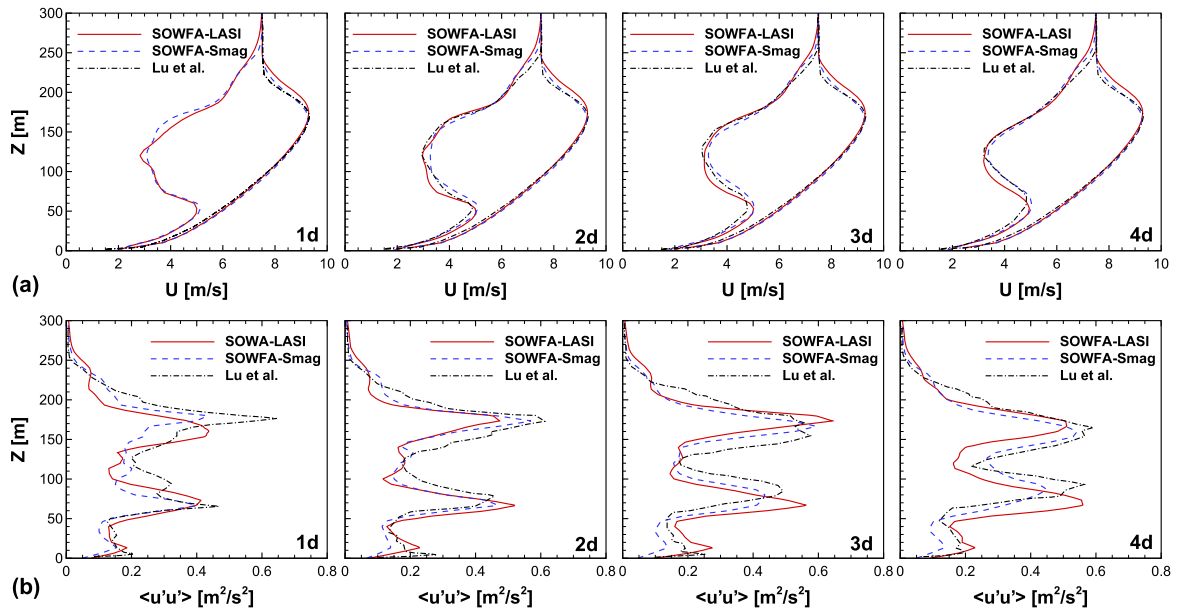

Figure 3. Stable windplant LES results at several locations downstream of the turbine. (a) Mean axial velocity and (b) TKE. Mean axial velocity from the precursor runs is also shown in (a). [Colour figure can be viewed at wileyonlinelibrary.com]

that the agreement between the TKE profiles obtained from the three simulations is reasonable. The constant-coefficient Smagorinsky result is closer to the reference LES result; however, the LASI model also gives very comparable results.

The newly developed version of SOWFA is thus able to qualitatively and quantitatively reproduce other stable ABL and stable windplant simulations and can be used for further advanced studies with confidence.

2.3. Simulation details

Twelve LES with differing stability conditions, layouts and wind directions are reported here. The simulations include the original Lillgrund layout with 48 Siemens 2.3 MW turbines (diameter $d = 93$ m and hub-height 63.4 m), arranged with a spacing of $4.3d$ along and $3.3d$ across columns (Figure 4(a)). A staggered layout obtained by shifting alternate rows by $1.6d$ across the columns was also investigated (Figure 4(b)). Note that rows A7-E36, A5-G45 and A3-G47 were shifted towards the north-west, while row A1-E31 was shifted in the opposite direction, towards south-west, to generate the staggered layout. The two prevailing wind directions at Lillgrund, southwest and northwest (225° and 315°, respectively), were combined with the original and staggered layouts to yield four wind farm configurations (called 225, 315, Stag-225 and Stag-315). These four configurations were studied under neutral, stable and unstable atmospheric conditions.

The simulation domain was a rectangular box of width 4 km each in the horizontal X and Y directions. The vertical extent was 1 km for the neutral and unstable cases and 500 m for the stable cases. The lateral walls were periodic, inflow or outflow, as explained later. Zero gradient and zero normal velocity conditions were applied at the top boundary. Wall models were applied to the bottom boundary with a surface roughness of 0.016 m. The thermal boundary condition at the bottom boundary was dependent on stability as follows: unstable conditions were induced by applying a heat flux of 0.04 K m s^{-1} while stable conditions by reducing the temperature of the bottom boundary at a rate of -0.25 K h^{-1}.

The numerical simulations followed a two-step methodology. The first step was the 'precursor' run, in which wind turbines were excluded, periodic conditions were applied to the lateral boundaries and the flow was driven by a uniform pressure gradient that was dynamically adjusted at each time step to maintain a wind speed of 9 m s^{-1} at 90 m height. The precursor runs were conducted for 12,000 s to set up a realistic turbulent ABL. Velocity and temperature fields at the inflow planes were stored over the next 2000 s for the neutral and stable cases and over the next 4000 s for the unstable cases. The inflow planes were south and west for the 225° cases and north and west for the 315° cases. The second step was the 'windplant' run, in which the turbines were introduced and non-periodic conditions were applied to the horizontal boundaries, with the fields stored during the precursor step applied at inflow boundaries. Simple zero pressure and zero normal derivatives of all other quantities at the outflow boundaries were found to be sufficient to ensure that the solution in the region of interest was not contaminated by artificial numerical reflection of waves from the outflow boundaries. Averages of turbulent statistics were computed over the last 1600 s for the neutral and stable cases and over the last 2000 s for the unstable cases. The instantaneous power generated by each turbine was computed by multiplying the shaft torque and the shaft rotational speed, as described in detail in Churchfield *et al.*[20] The shaft torque was obtained from the blade aerodynamic forces computed by the actuator-line model. The shaft rotation speed was obtained on the basis of a torque-controller algorithm[20] and was a function of the moment of inertia of the rotor and the shaft torque. All parameters
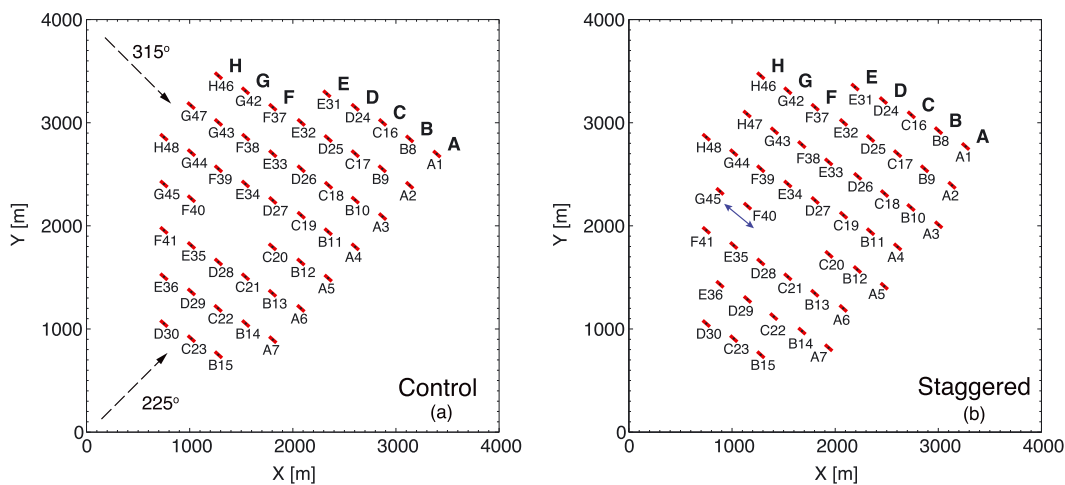

Figure 4. Plan views of the (a) original and (b) staggered Lillgrund wind farm layouts. Turbines are denoted by short lines and are arranged in columns A–H. Arrows denote the two wind directions simulated. The blue arrow upstream of turbine F40 in (b) marks the axis Y_r and the location investigated in Figure 11(d). [Colour figure can be viewed at wileyonlinelibrary.com]

were uniform across all runs so as to ensure fair comparison of the power values computed in the different cases. The instantaneous power was averaged in time, similar to the averaging performed for all turbulent quantities. Time variation of the horizontally averaged surface friction velocity and the power generated by the turbines indicated that the durations simulated were adequate for the simulations to reach quasi-stationary states and for the statistics to converge.

Following Churchfield *et al.*,[20] the grid resolution was 7 m in each direction for all precursor simulations. For neutral and unstable windplant simulations, a refinement region surrounding the turbines was introduced,[13] with 3.5 m resolution. The stable windplant simulations were conducted with uniform resolutions of 5 m in the horizontal directions and 4.17 m in the vertical direction. This ensured approximately 25 grid points in the rotor region, which were sufficient to capture the unsteady effects of wind turbines.[13] The total grid sizes were approximately 47 million computational cells for the precursors, approximately 83 million for the neutral and unstable windplant simulations and approximately 77 million for the stable windplant simulations.

The simulations were carried out on the University of Delaware's Mills HPC cluster, typically using 192 processors, with approximately 100,000 and 60,000 CPU hours, respectively, for the precursor and windplant simulations.

3. RESULTS

3.1. Precursor ABL simulations

Precursor simulation results under neutral, stable and unstable conditions are described first. The neutral profile of time- and horizontally averaged horizontal wind speed followed the expected logarithmic law of the wall, while the unstable and stable profiles deviated from the log-law because of buoyancy (Figure 5(a)). The mean horizontal velocity profiles agree well with the velocity profiles predicted on the basis of the MOST in the surface layer close to the wall.[25] Since the wind speeds at $Z = 90$ m were forced to be equal across all simulations, wind shear in the rotor region, geostrophic wind and surface properties were different under different stabilities. Shear and geostrophic wind were strongest in the stable cases
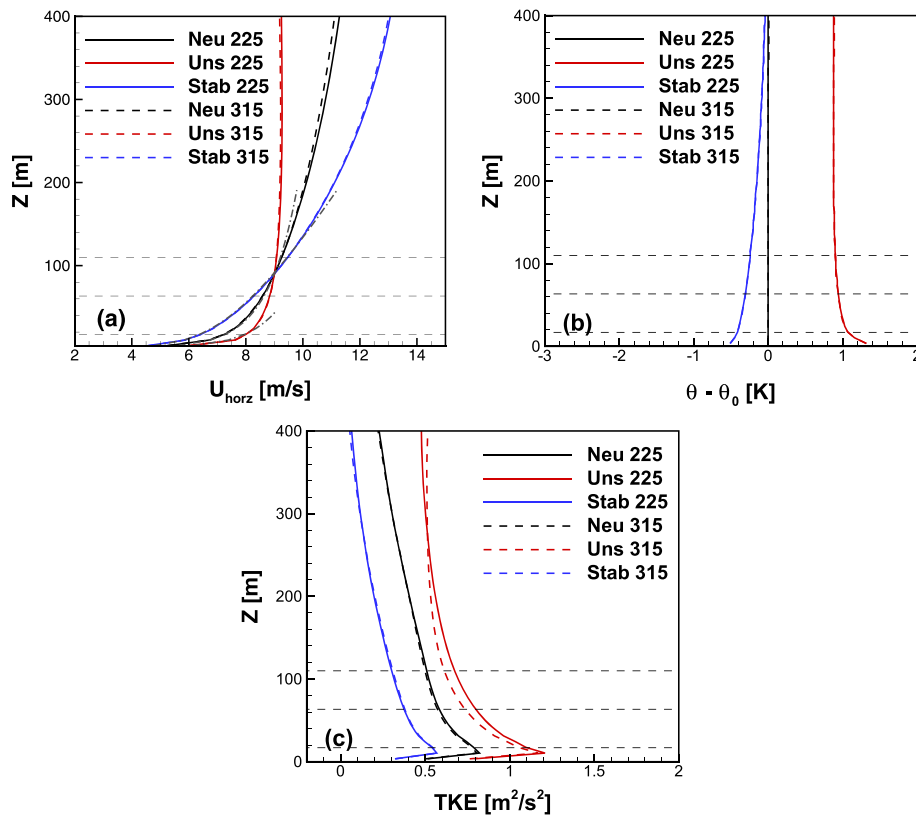

Figure 5. Vertical profiles of time and horizontally averaged (a) horizontal velocity, (b) potential temperature differential and (c) TKE from the precursor runs. The dashed horizontal lines represent the tip–top, hub and tip–bottom heights. The dash-dotted lines in (a) denote predictions of the MOST.[25] [Colour figure can be viewed at wileyonlinelibrary.com]

and weakest in the unstable cases. Surface friction velocities were approximately 0.45, 0.38 and 0.33 m s^{-1} in the unstable, neutral and stable cases, respectively. At all vertical levels, turbulence was highest in the unstable cases and lowest in the stable cases (Figure 5(c)), as expected.[19] The turbulence intensities at the hub-height were 9.2%, 6.8% and 4.6% in the unstable, neutral and stable cases, respectively.

Potential temperature was uniform in the neutral cases, decreased with height in the unstable cases and increased with height in the stable cases (Figure 5(b)). In the unstable ABL cases, the potential temperature gradient was large only near the wall, while the change in the temperature over the turbine rotor region was very small, indicating that the fluid was well mixed because of the action of turbulence. The stable cases maintained an almost constant rate of decay of potential temperature throughout much of the domain. Obukhov lengths, characterizing the strengths of the stabilities, were −172 and 263 m for the unstable and stable cases, which can hence be classified as moderately unstable/stable following Wharton and Lundquist.[26]

Finally, results of the precursor simulations with the wind from south-west and north-west were almost identical to each other, except for small differences in the unstable TKE profiles (less than 7%). This implies that the differences observed between the various windplant simulation results shown in Section 3.3 were not due to differences in the incoming wind.

It should be noted that since the wind speeds at 90 m were kept fixed across all runs, the wind speeds at hub-height differed with stability. For a given velocity profile, the 'power potential' was calculated as the integral $\int (1/2)U_{\mathrm{horz}}^3 dA$ over the rotor-disk region. The power potentials of the unstable and stable precursor profiles were found to vary by approximately +9% and −9%, respectively, over the power potential of the neutral precursor profile. This indicates that an isolated turbine, operating under the unstable conditions depicted in Figure 5(a), is expected to produce 9% more power than the one operating under neutral conditions shown in Figure 5(a). Similarly, an isolated turbine exposed to the stable profiles in Figure 5(a) would produce 9% less power than a turbine operating under the neutral conditions imposed here. As discussed in Section 3.3, these differences between the precursor profiles of the incoming wind were accounted for by comparing relative powers instead of the total powers.

3.2. Wind farm simulations

Results of the Lillgrund wind farm simulations are discussed next. For further validation of the windplant component and power computation algorithm of SOWFA, LES results for all stabilities using the control layout are compared with observational data taken at Lillgrund. In addition to the southwesterly (225°) and northwesterly (315°) winds described previously, additional simulations corresponding to westerly winds (270°) were conducted under neutral, stable and unstable conditions and compared with the observations.

The proprietary dataset, provided by Vattenfall, included wind power, yaw angle, wind speed, rotational speed and blade pitch angles for all 48 turbines for approximately 16 months at a frequency of 1 min or less. Although meteorological data from a mast located approximately 250 m to the southwest of the farm were available, they were not used here because of the limited range of undisturbed wind directions and the poor maintenance record, reported already in the literature.[15,27,28] No information on stability or turbulence intensity was available. Following Creech *et al.*,[28] the yaw angle, also known as the nacelle direction, was used here as a proxy for wind direction, after proper bias removal.

The process of yaw bias removal consisted of multiple steps, summarized later, with the overarching goal of producing meaningful wind power statistics for comparisons with LES. The first step composed of general quality checks to remove unrealistic values on the basis of the 2.3 MW Siemens turbine specifications[29] and curtailed conditions. Next, directions of alignment of the turbines (e.g., 0°, 42° and 75°) and a representative pair of front-row and second-row turbines for each direction of alignment (e.g., turbines A3 and B10 for 120° and C23 and C22 for 222°) were identified. The median of all the turbines' yaw angle was used as a proxy for the wind direction over the whole farm at each time instant. For each direction of alignment, the relative power (i.e., power of the second-row turbine divided by that of its corresponding first-row turbine) was computed for all time instants when the yaw angle was within a range of 20° around the direction of alignment. An example of the cloud of observed values of relative power is shown in Figure 6 for turbines T22 and T23 for wind directions around 222°. The minimum of the relative power must naturally occur at the direction of alignment (222°, in the present case), but it was always found to be off by some amount. The yaw bias could be determined as the difference between the position of the observed minimum of the relative power and the direction of alignment. However, since the relative power data as a function of direction were highly scattered, a Gaussian fit through the median values of relative power was used to smooth the data before identifying the minimum. This procedure yielded a yaw bias of 4.76° (i.e., difference between the diamond and the star) in Figure 6. Yaw biases for wind directions in between two directions of alignment were determined by linear interpolations. Finally, the turbine yaw angles were corrected by applying the yaw bias correction so identified and the median yaw angle that was used as a proxy for the wind direction.

The wind speed measured by the nacelle anemometer of the turbines, typically a very noisy and unreliable measurement, was used only to select observed values for which the nacelle wind speeds was 5–12 m s^{-1}, the range in which the power curve of the 2.3 MW Siemens turbine is basically linear. Also, in this range, the relative power is independent
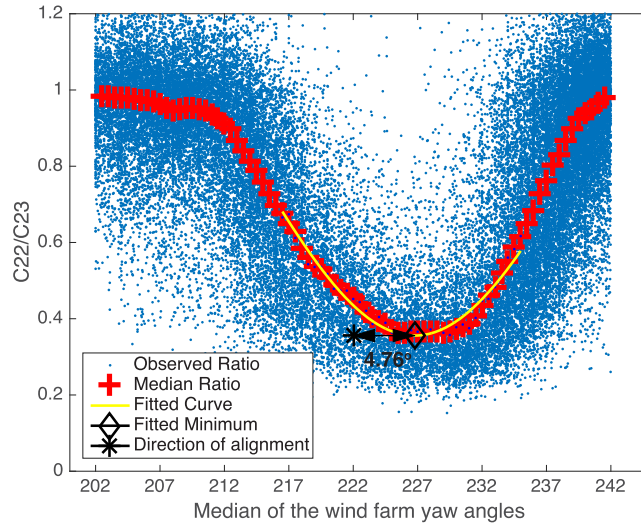
Figure 6. Observed relative power (power of turbine C22 over power of front-row turbine C23) for median yaw angle, a proxy for wind farm wind direction, of approximately 222°. The median of relative power is indicated by a red plus sign, the Gaussian fit by a yellow line, the minimum of the Gaussian fit by a diamond, the expected minimum by a star and the yaw bias by a dual-head arrow.
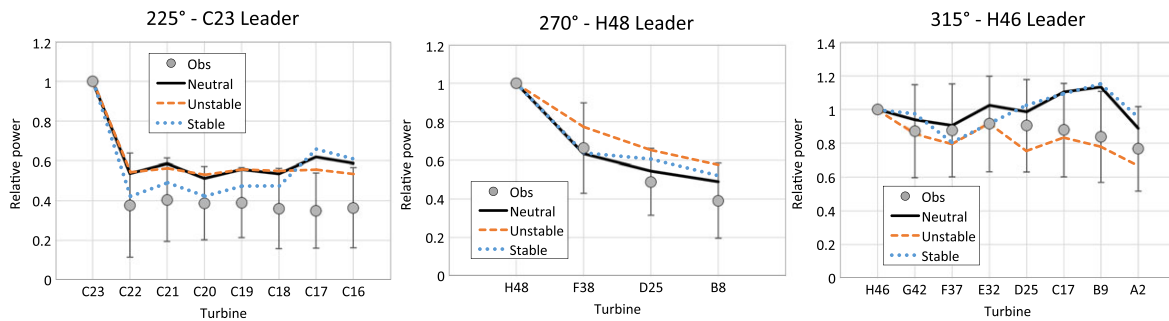

Figure 7. Observed and simulated relative power at selected wind turbine columns for the three wind directions of interest. [Colour figure can be viewed at wileyonlinelibrary.com]
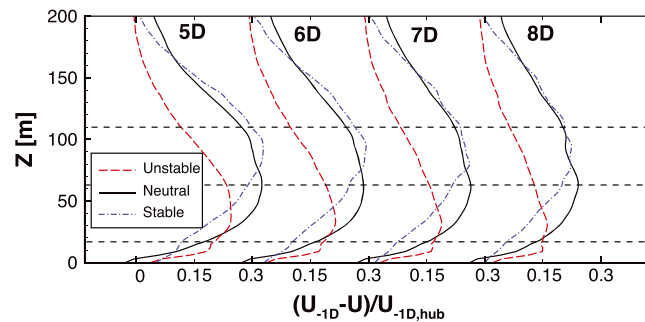

Figure 8. Velocity deficit profiles five to eight diameters downstream of turbine A1 in the 225 configuration under neutral (black lines), unstable (red lines) and stable (blue lines) conditions. The dashed black horizontal lines indicate tip–top, tip–bottom and hub-height locations. U_{-1d} denotes the velocity profile one diameter upstream of the first turbine in the column of turbine A1 (i.e., turbine A7) and $U_{-1d,\text{hub}}$ denotes the velocity at the hub-height at that location. [Colour figure can be viewed at wileyonlinelibrary.com]

of wind speed,[28] which supports the generality of the LES simulations conducted here for a fixed 90 m wind speed of $9\ \mathrm{m\ s^{-1}}$.

After the quality checks and yaw bias correction described earlier, observed relative power can be computed for the three relevant wind directions studied here and compared with that from the unstable, neutral and stable SOWFA results. For the three wind directions of interest here (225°, 270° and 315°), SOWFA results compare favorably against the observations (Figure 7), as the greatest majority of SOWFA cases are within one standard deviation of the observations and follow the observed pattern of drop-in relative power between the leader and the other turbines, for all atmospheric stabilities.

Some qualitative features of the wakes downstream of turbine A1 are seen in Figure 8. The wake is shortest under unstable conditions and longest under stable conditions. The locations of the peaks of the velocity deficit profiles are different under different stabilities. The peaks are found to be close to the hub-height under neutral conditions, below the hub-height under unstable conditions and above the hub-height under stable conditions. The same qualitative features were noted in an LES study of an isolated turbine under unstable, neutral and stable conditions by Abkar and Porté-Agel.[9] Turbine A1 was chosen here because this turbine is on the edge of the wind farm and hence displays qualitative similarities to an isolated turbine.

The successful comparisons with field observations and previous LES study indicate that SOWFA can be trusted to provide the correct physical flow patterns inside the wind farm and realistic power generation.

3.3. Total and relative power

The total power generated by the 12 configurations studied are plotted in Figure 9(a). The windplant LES results show that in all cases with wind from 225°, staggering increased the power generated drastically. This result was reported previously in Archer *et al.*[13] for neutral conditions. A similar increase in power with staggering rows normal to the wind in a miniature wind farm was also reported in Wu and Porté-Agel.[30] The power generated in all cases with wind from 315° was much greater than in the 225° cases. However, with wind from 315°, the staggered layout yielded slightly less power than the original layout. These trends are explained in Section 3.4.

The effect of stability on wind farm performance can be gleaned by comparing the power generated under neutral, stable and unstable conditions for a fixed layout (Figure 9(a)). For all layouts, the power generated under unstable conditions was larger than under neutral conditions. The increase ranged from approximately 3% for the 315 configuration to almost 12% between the Stag-225 cases. Changing the atmospheric conditions from neutral to stable results in different behavior of the wind farm under different configurations. Three out of four configurations showed less power under stable conditions than under neutral conditions. This drop was as large as 19% for 225 and approximately 5–7% for 315 and Stag-315 configurations. In contrast, the Stag-225 configuration exhibited a slight (1.5%) increase in power under stable compared with neutral conditions.

In order to quantify the wake losses in the windplant configurations, the relative powers obtained from the 12 simulations are plotted in Figure 9(b). Relative power was defined here as the total power normalized by the number of turbines times the power of an upstream 'undisturbed' turbine. The average of the powers of turbines B15, C23 and D30 was used for the normalization for the 225 and Stag-225 configurations. Similarly, results of simulations of 315 and Stag-315 configurations were normalized by the average of the powers of turbines H46, H47 and H48. For a given configuration, these front-row average power values varied by around 9% between neutral and stable, and neutral and unstable conditions.
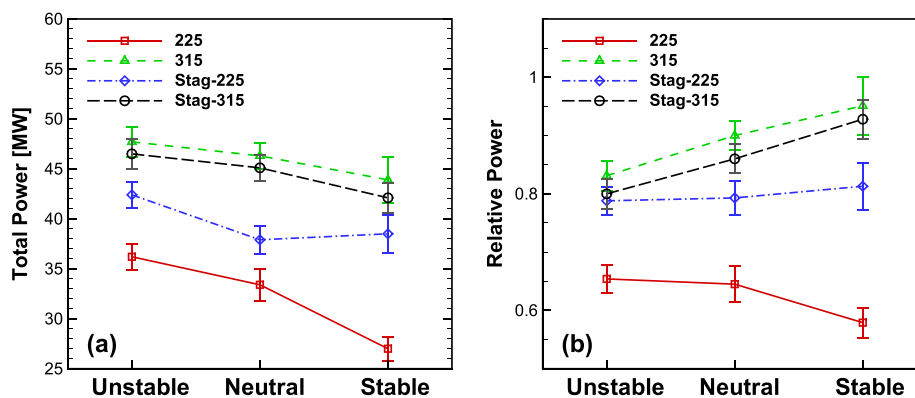

Figure 9. (a) Total power generation and (b) relative power from the windplant simulations. Symbols denote time-averaged values, and error bars denote standard deviations. Relative powers were determined by normalizing the total power with averages of powers of B15, C23 and D30 for the 225 cases and H46, H47 and H48 for the 315 cases. [Colour figure can be viewed at wileyonlinelibrary.com]

This is in keeping with the differences in the power potentials of the precursor profiles, noted in the previous subsection. The front-row averages varied by about 3.5%, 4.1% and 1.8% between the different configurations, for unstable, neutral and stable conditions, respectively. While some of the differences in trends between the total and relative power values can be partially attributed to variability in the front-row averages used for normalization, we note that this variability is significantly smaller than the differences observed in the total power values.

Figure 9(b) shows that the effect of configuration on relative power was similar to that on the total power. The effect of stability, on the other hand, was qualitatively different for different configurations. For the 225 configuration, the relative power was larger under unstable conditions and smaller under stable conditions than under neutral stability. For the 315 and Stag-315 configurations, the opposite trend was observed, namely, relative power was largest for stable conditions and smallest for unstable conditions. The relative power in the Stag-225 configuration seemed more or less independent of the
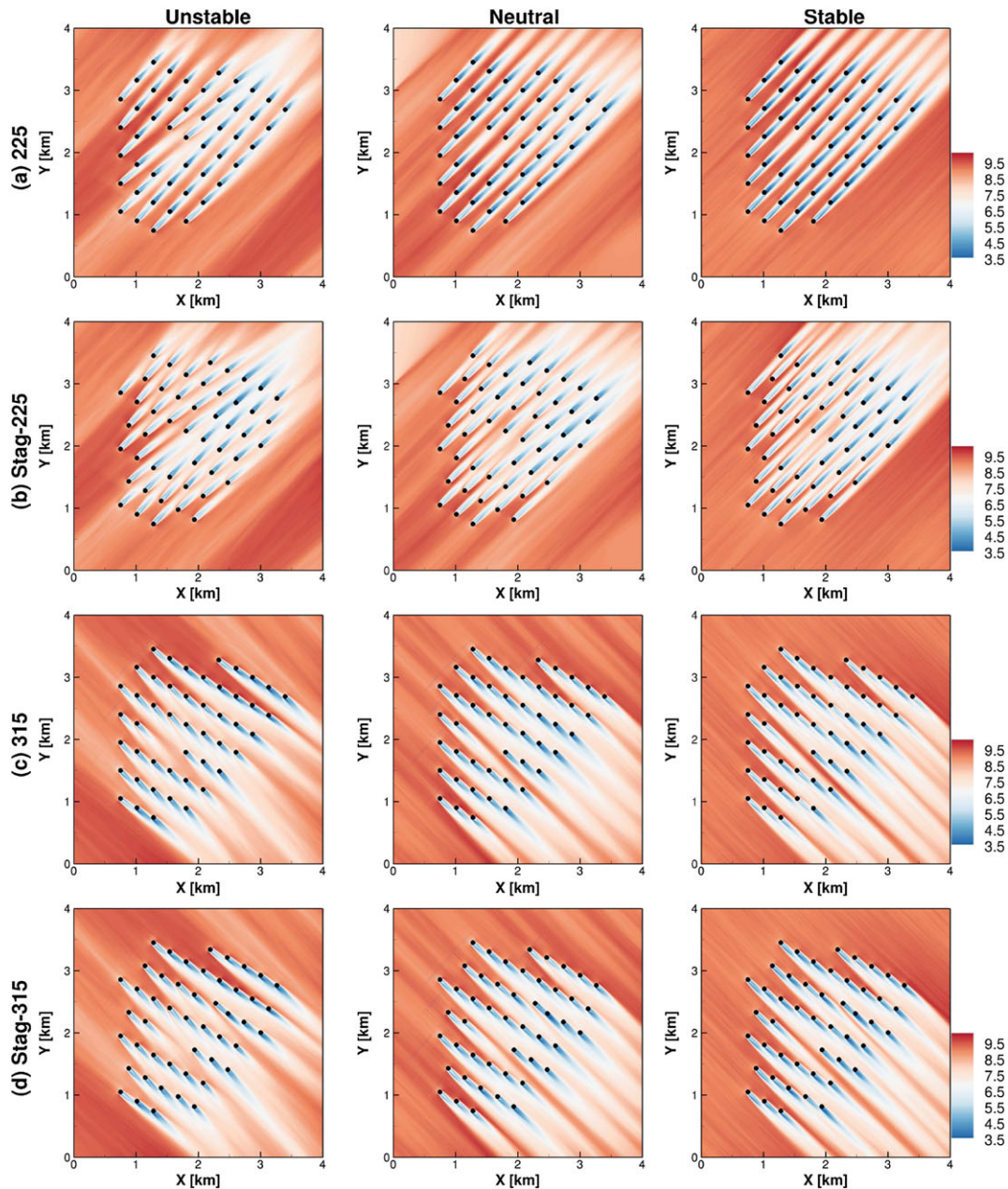

Figure 10. Time-averaged horizontal velocity contours at $Z = 90$ m in (a) 225, (b) Stag-225, (c) 315 and (d) Stag-315 windplant configurations under unstable (left), neutral (center) and stable (right) conditions.

stability conditions, although with a very slight trend similar to the 315 and Stag-315 configurations. The relative power is inversely related to wake losses, and the results in Figure 9(b) point to complicated interactions between wind farm configuration and stability, which are explained in Section 3.5.

The wakes behind each turbine are apparent as regions of reduced velocity magnitude in Figure 10. The wake characteristics depend on wind direction and stability, and the interactions between turbine wakes determine the total power generated in each case. A number of different features of these wakes are apparent. They were shortest in unstable cases and longest in stable cases. The lateral spread was largest in unstable cases (wakes were more diffuse) and smallest in stable conditions (sharp, crisp wakes). As a result, clearly defined 'channels' of high-velocity regions were seen (compare 225 configurations) to a greater degree in stable cases as compared with neutral and unstable cases. These features are further analyzed in Section 3.5.

3.4. Effect of configuration

The effect of configuration (i.e., layout and wind direction) on the power generation can be explained on the basis of the geometric blockage of some of the turbines in the wind farm. The columns and rows of Lillgrund made angles of 221.8° and 300°, respectively, to the north. For the 225 configuration, very few turbines (e.g., B15, C23 and D30) were exposed to the undisturbed wind, while most of the turbines lay directly in the wakes of upstream turbines (Figure 10). As a result, significant power potential was lost to wake losses in these cases, irrespective of the stability conditions. Staggering increased the number of turbines exposed to the undisturbed incoming wind and reduced the wake losses of downstream turbines, since the increased streamwise spacing between the turbines allowed for recovery of the velocity profiles.

The increased power generation for the 315 cases can be explained similarly. In the 315 configuration, the wind was not aligned to the columns but made an angle of approximately 15°. As a result, a large number of turbines were exposed to the undisturbed wind, free of the effects of the wakes of any upstream turbines. Wake losses were further reduced since the wakes of upstream turbines have much longer distances to recover before a downstream turbine was encountered. These trends of power with wind farm configuration held for all three stabilities, although with different magnitudes.

3.5. Effect of stability

As noted previously in Section 3.3, the effect of stability on wake losses was found to be inconsistent across different configurations (Figure 9(b)). The horizontal velocity contour plots in Figure 10, and profiles of velocity and TKE at various locations in the wind farms, shown in Figure 11, are used to extract three competing effects that can be used to explain the seemingly inconsistent response of the wind farm to changes in stability.
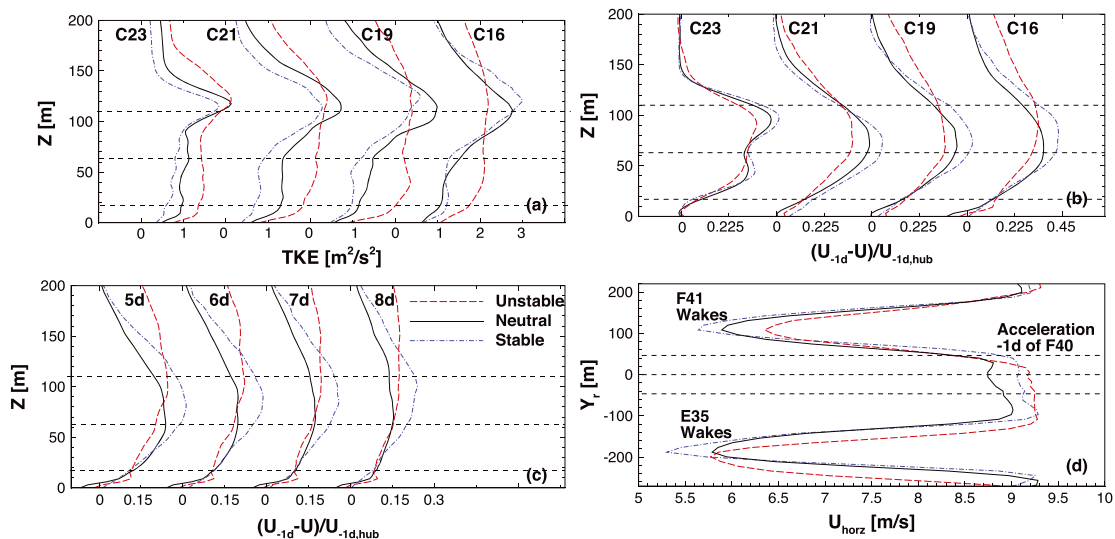

Figure 11. Vertical profiles of (a) TKE and (b) normalized velocity deficits $3d$ downstream of several turbines in column C of the 225 configuration. (c) Vertical profiles of normalized velocity deficits at several locations downstream of turbine C16 in 225 configuration. (d) Lateral profiles along the line shown in Figure 4(b) $1d$ upstream of turbine $F4$ in Stag-225 configuration. The dashed horizontal lines represent the rotor-center and rotor-tip locations. U_{-1d} denotes the velocity one diameter upstream of turbine C23 and $U_{-1d,hub}$ denotes the velocity one diameter upstream of turbine C23 at the hub-height. [Colour figure can be viewed at wileyonlinelibrary.com]

1. TKE and rate of recovery of velocity deficits: The power generated by downstream turbines depends on how quickly the velocity profiles recover their original shape, which in turn depends on TKE. Figure 11(a) shows that in general, except for a region close to the top–tip height, TKE values were larger under unstable conditions than in neutral conditions. Higher TKE levels were representative of more energetic eddies that lead to more efficient mixing of higher momentum from aloft into the wake region. Increased TKE levels thus led to faster recovery of the wakes, as seen in the velocity deficit profiles along column C of the wind farm, plotted in Figure 11(b). Figure 11(c) shows that the velocity deficits are smaller under unstable conditions, even downwind of the wind farm. This indicated that array losses were reduced in the unstable cases. Conversely, TKE was lower under stable than neutral conditions, especially downstream of the first three turbines in column C, which slowed down the rate of wake recovery and led to higher deficits and increased wake losses. The differences between the rates of wake recovery under unstable, neutral and stable conditions are also seen clearly in Figure 10(a).

2. Lateral spread of wakes: The contour plots of Figure 10 show that, irrespective of the wind farm layout and wind direction, the lateral spread of wakes was enhanced under unstable conditions, compared with neutral conditions. This was because the larger TKE levels present in unstable conditions that led to more efficient mixing of momentum from aloft also led to more efficient mixing in the lateral directions. Conversely, lower TKE levels under stable conditions, as compared with neutral conditions, led to suppressed mixing in the lateral direction in addition to suppressing mixing in the vertical direction. Comparing the neutral and stable cases displayed in Figure 10, it is clear that the lateral spread of wakes was smaller under stable conditions than under neutral conditions.

3. Acceleration between adjacent wakes: Velocity profiles in the Stag-225 configuration along the line marked in Figure 4(b) were extracted and plotted in Figure 11(d). It is clear that the velocity reduced downstream of turbines E35 and F41. On account of mass conservation, the velocity in the region between the two wakes and upstream of turbine F40 increased, compensating for the velocity deficits in the wakes of turbines E35 and F41. The magnitude of this acceleration was larger in the stable case than in the neutral case. As a result, the power produced by turbine F40 was larger in the stable case as compared with the neutral case, and by contrast, the wake losses were smaller under stable conditions than under neutral conditions.

The aforementioned three effects can be used to qualitatively explain the differing effects of stability for different configurations on the wake losses. Most of the turbines in the 225 configuration lay directly in the wakes of upstream turbines. For this configuration, the wake losses were controlled primarily by the rate of wake recovery, and hence, the relative power was larger under unstable conditions and smaller under stable conditions than under neutral conditions. For the 315 and Stag-315 configurations, the downstream turbines were very rarely located directly behind upstream turbines. Thus, the power of the downstream turbines was primarily affected by the lateral spread of wakes. As a result, the relative power was largest under stable conditions (since the lateral spread of wakes was smallest) and smallest under unstable conditions (since the lateral spread was largest). For the Stag-225 configuration, the slower wake recovery under stable conditions tended to increase wake losses, while the acceleration between adjacent upstream wakes tended to reduce wake losses, over neutral conditions. These effects were almost evenly balanced and that led to overall wake losses that were independent of stability for the Stag-225 configuration.

3.6. Implications for analytical models

The two analytical models of wind farms that are most widely used and that form the basis of many others are the Jensen/PARK model[31] and the top–down model.[32] This LES study indicates that both models ignore important features of the flow in finite-sized wind farms. The PARK model accounts for velocity deficits downstream of turbines but does not consider accelerations at the edges of the wakes, which can lead to increased power under stable conditions for certain configurations (e.g., in the Stag-225 configuration). The top–down model assumes that the details of the horizontal layout are not important and that the product of the spacings in the streamwise and spanwise directions alone is sufficient to predict the velocity in the wind farm. Our LES show that this is untrue, since the results are significantly different when the stability is kept unchanged but the wind direction and/or staggering are changed.

4. CONCLUSIONS

The LES of wind farms with aligned and staggered layout of turbines were conducted under three atmospheric stabilities and two wind directions using NREL's SOWFA code. For a given stability, the power generated by the 225 configuration was smallest, followed by Stag-225, Stag-315 and 315, in that order. The effect of configuration can be explained by the extent to which upstream turbines block downstream turbines and the distance available for wakes to recover the velocity deficits.

The response of the wind farm to changes in stability is harder to explain, since it is complicated by the interactions between three competing effects. First, the turbulence intensity level dictated the rate of vertical mixing of momentum and resulting wake recovery. Unstable conditions led to faster vertical mixing and hence faster recovery of velocity deficits than neutral and stable conditions. Second, the lateral spread of wakes was largest under unstable conditions and smallest under stable conditions. Last, regions in the wind farm experienced accelerations in velocity because of the presence of adjacent upstream wakes. These accelerations were larger in stable cases and smaller in neutral cases, leading to the possibility of increased power in stable cases if a turbine were to lie in such a region. The 225 configuration, with the columns aligned with the wind, was affected primarily by the rate of vertical mixing of momentum and hence yielded largest wake losses in stable conditions and smallest wake losses under unstable conditions. The 315 and Stag-315 configurations were affected primarily by the lateral spread of wakes and hence showed the opposite trend. The competing effects almost balanced each other in the Stag-225 configuration, and hence, no significant differences were observed in wake losses in this configuration with stability.

These results indicate that the power generated by wind farms is a complicated function of layout, wind direction and stability under very similar wind speeds and point to the deficiencies in the existing PARK and top–down models. In particular, PARK models need to account for accelerations at the edges of the turbine wakes, while top–down models need to account for details of the horizontal layouts of turbines to be applicable to finite-sized wind farms. Future efforts will focus on the use of these LES results towards the evaluation of less expensive models such as those based on Reynolds-averaged Navier–Stokes turbulence closures; parabolized Navier–Stokes equations; and simplified, analytical, physics-based and statistical wake models that account for the effects of stability on the power generation of wind farms.

ACKNOWLEDGEMENTS

REFERENCES

1. Wharton S, Lundquist JK. Atmospheric stability affects wind turbine power collection. *Environmental Research Letters* 2012; **7**: 014005.
2. Vanderwende BJ, Lundquist JK. The modification of wind turbine performance by statistically distinct atmospheric regimes. *Environmental Research Letters* 2012; **7**: 034035.
3. Wharton Sonia, Lundquist JK, Marjanovic N, *Synergistic effects of turbine wakes and atmospheric stability on power production at an onshore wind farm*, Technical Report LLNL-TR-524756, Lawrence Livermore National Laboratory, 2012.
4. Hasager CB, Giebel G, Technical Report D7.20, The European Energy Research Alliance Design Tools for Offshore Wind Farm Cluster, 2015.
5. Peña A, Réthoré P-E, Rathmann O. Modeling large offshore wind farms under different atmospheric stability regimes with the PARK wake model. *Renewable Energy* 2014; **70**: 164–171.
6. Peña A, Rathmann O. Atmospheric stability-dependent infinite wind-farm models and the wake decay coefficient. *Wind Energy* 2014; **17**: 1269–1285.
7. Bhaganagar K, Debnath M. Implications of stably stratified atmospheric boundary layer turbulence on the near-wake structure of wind turbines. *Energies* 2014; **7**: 5740–5763.
8. Bhaganagar K, Debnath M. The effects of mean atmospheric forcings of the stable atmospheric boundary layer on wind turbine wake. *Journal of Renewable and Sustainable Energy* 2015; **7**: 013124.
9. Abkar M, Porté-Agel F. Influence of atmospheric stability on wind-turbine wakes: a large-eddy simulation study. *Physics of Fluids* 2015; **27**: 035104.
10. Lu H, Porté-Agel F. Large-eddy simulation of a very large wind farm in a stable atmospheric boundary layer. *Physics of Fluids* 2011; **23**: 065101.
11. Abkar M, Porté-Agel F. The effect of free-atmosphere stratification on boundary-layer flow and power output from very large wind farms. *Energies* 2013; **6**: 2338–2361.
12. Lu H, Porté-Agel F. On the impact of wind farms on a convective atmospheric boundary layer. *Boundary-Layer Meteorology* 2015; **157**: 81–96.

13. Archer CL, Mirzaeisefat S, Lee S. Quantifying the sensitivity of wind farm performance to array layout options using large-eddy simulation. *Geophysical Research Letters* 2013; **40**: 4963–4970.

14. Porté-Agel F, Wu Y-T, Chen C-H. A numerical study of the effects of wind direction on turbine wakes and power losses in a large wind farm. *Energies* 2013; **6**: 5297–5313.

15. Dahlberg J, *Assessment of the Lillgrund windfarm*, Technical Report 6_1 LG Pilot Report, Vattenfall Vindkraft AB, 2009.

16. Bergström H, *Meteorological conditions at Lillgrund*, Technical Report 6_2 LG Pilot Report, Vattenfall Vindkraft AB, 2009.

17. Meneveau C, Lund T, Cabot W. A Lagrangian dynamic subgrid-scale model of turbulence. *Journal of Fluid Mechanics* 1996; **319**: 353–385.

18. Etling D. *Modelling the Vertical ABL Structure. Modelling of Atmospheric Flow Fields*. chap. 2. World Scientific Publishing: Singapore, 1996,45–86.

19. Stull RB. *An Introduction to Boundary Layer Meteorology*. Kluwer Academic Publishers: The Netherlands, 1988.

20. Churchfield MJ, Lee S, Moriarty PJ, Martinez LA, Leonardi St, Vijaykumar G, Brasseur JG. A large-eddy simulation of wind-plant aerodynamics. *Technical Report NREL/CP-5000-53554.* National Renewable Energy Laboratory, 2012.

21. Churchfield MJ, Lee S, Michalakes J, Moriarty PJ. A numerical study of the effects of atmospheric and wake turbulence on wind turbine dynamics. *Journal of Turbulence* 2012; **13**: 1–32.

22. Churchfield MJ, Lee S, Moriarty PJ. Adding complex terrain and stable atmospheric condition capability to the simulator for on/offshore wind farm applications (SOWFA). *National Renewable Energy Laboratory*, 2013.

23. Churchfield MJ. *A description of the OpenFOAM Solver boussinesqBuoyantPisoFOAM*, 2010. Available online at http://openfoamwiki.net/index.php/BuoyantBoussinesqPisoFoam (Accessed 25 January 2017).

24. Beare RJ, Macvean MK, Holtslag AM, Cuxart J, Esau I, Golaz J-C, Jimenez M, Khairoutdinov M, Kosovic B, Lewellen D. An intercomparison of large-eddy simulations of the stable boundary layer. *Boundary-Layer Meteorology* 2006; **118**(2): 247–272.

25. Businger JA, Wyngaard JC, Izumi Y, Bradley EF. Flux–profile relationships in the atmospheric surface layer. *Journal of Atmospheric Sciences* 1971; **28**: 181–189.

26. Wharton S, Lundquist JK. Assessing atmospheric stability and its impacts on rotor-disk wind characteristics at an onshore wind farm. *Wind Energy* 2012; **15**: 525–546.

27. Iliev S. Array losses and array benefits: the atmospheric blockage effect at offshore wind parks, *Master's Thesis*, Delft University of Technology, 2014.

28. Creech A, Früh W-G, Maguire E. Simulations of an offshore wind farm using large-eddy simulation and a torque-controlled actuator disc model. *Surveys in Geophysics* 2015; **36**: 427–481.

29. Siemens. *Siemens wind turbine SWT-2.3-93*, 2009. Available at http://www.energy.siemens.com/us/pool/hq/power-generation/wind-power/E50001-W310-A102-V6-4A00_WS_SWT-2.3-93_US.pdf, Accessed 25 January 2017.

30. Wu Y-T, Porté-Agel F. Simulation of turbulent flow inside and above wind farms: model validation and layout effects. *Boundary-Layer Meteorology* 2013; **146**: 181–205.

31. Katic I, Hojstrup J, Jensen NO. A simple model for cluster efficiency. *European Wind Energy Association Conference and Exhibition*, Rome, Italy, 1986. October 7-9.

32. Calaf M, Meneveau C, Meyers J. Large eddy simulation study of fully developed wind-turbine array boundary layers. *Physics of Fluids* 2010; **22**: 015110.